An investigation on the mechanism of droplet formation in a microfluidic T-junction

An investigation on the mechanism of droplet formation in a microfluidic T-junction

J. Sivasamy, T.-N. Wong*, N.-T. Nguyen

School of Mechanical and Aerospace Engineering, Nanyang Technological University, 50 Nanyang Avenue, Singapore 639798, Singapore

**e-mail: mtnwong@ntu.edu.sg*

J. Sivasamy, L. T.-H. Kao

*Institute of Microelectronics, A*STAR (Agency for Science, Technology and Research), 11 Science Park Road, Singapore Science Park II 117685, Singapore*

Abstract This paper reports the findings of a numerical investigation on the droplet break-up in a microfluidic T-junction. The numerical flow visualization of the droplet formation process is validated with the experimental flow visualization. From the computational results, we show that the pressure profile of the dispersed phase and the continuous phase in the squeezing regime changes as the droplet break-up process proceeds. The assumption taken by other researchers that the dispersed phase pressure profile, during the droplet formation process at a T-junction, remains constant and only the continuous phase pressure changes according to the blockage of the channel is proved to be invalid. We provide new insights on the pressure difference between the dispersed phase and the continuous phase during the droplet break-up process and show that the minimum pressure difference happens at the last moment of the droplet break-up and not during the second and third stage of the droplet formation mechanism in the squeezing regime as suggested by other researchers.

Keywords Droplet microfluidics ·Droplet break-up mechanism ·Microfluidic T-

junction ·Multiphase flow

1 Introduction

Due to the small size (in the order of 10–100μm) and low flow rates (few μl/s), flows in microfluidic systems are generally dominated by viscous effects. Consequently, the laminar flow and high Péclet number, the two main characteristics of microflows, allow the transport of chemical substances in the microchannels in a controlled manner, both in space and time (Stone et al. 2004; Squires and Quake 2005). There has been a growing interest in droplet-based microfluidic systems because they are useful as sample transporters, mixing enhancers, dispersion eliminators, and simply good discrete microreactors (Gunther et al. 2004, 2005; Muradoglu and Stone 2005; Song et al. 2006; Bringer et al. 2004;Teh et al. 2008). Aqueous droplets in microchannel are generated in an immiscible carrier fluid using T-junction and the process of droplet formation in microfluidic channels has received significant attention over the last decade (Thorsen et al. 2001; Song et al. 2003; Gunther et al. 2004; Stone et al. 2004; Guillotand Colin 2005; Nisisako et al. 2005; Utada et al. 2005; Zheng and Ismagilov 2005; Garstecki et al. 2006; Sivasamy et al. 2010).

Thorsen et al. (2001) first observed the formation of aqueous droplets in oil in microchannels. The authors suggested that the dynamics of droplet formation is dominated by the balance of tangential shear stresses and interfacial tension (i.e., the capillary number). Tice et al. (2004) characterized the experimental conditions required to form nano-liter sized droplets of viscous aqueous reagents in flows of immiscible carrier fluid within microchannels. They reported that plugs formed reliably in a flow of water-immiscible carrier fluid for capillary number less than 0.01. Garstecki et al. (2006) described the process of formation of droplets and bubbles in a microfluidic T-junction. They identified that at low capillary numbers break-up is not dominated by shear stress but by the pressure drop—the dominant contributor to the dynamics of break-up—across the emerging droplet and named the mechanism as squeezing. They argued that this mechanism is directly connected to the confined geometry in which the drop is formed and proposed a scaling law for the size of the droplets that is based only

on the ratio of flow rates of the two immiscible liquids and independent of the value of the capillary number.

De Menech et al. (2008) identified, through a numerical investigation of the dynamics of break-up of immiscible fluids at a microfludic T-junction, three distinct regimes of formation of droplets: squeezing, dripping, and jetting. They used the phase-field model to numerically compute the pressure, droplet volume, and droplet radius and based on the observation they identified the three regimes in the dynamics of droplet break-up. Christopher and co-workers (2008) reported a systematic experimental study of droplet break-up at T-shaped microfluidic junctions for conditions near the transition from squeezing dominated to dripping, where the viscous stresses become important. They described the complicated process based on two dimensionless parameters: the capillary number and the flow rate ratio. Xu et al. (2008) proposed correlations for droplet formation in T-junction ranging from squeezing to dripping and developed a modified capillary number for the continuous phase by using the local continuous phase flow rate at the droplet formation site. Long Sang and Wang (2009) studied the effect of viscosity, for both Newtonian and power law fluids, on droplet formation in T-shaped microchannels by analytical and numerical methods. Liu and Zhang (2009) performed a numerical study using phase-field model to describe fluid/fluid interfacial dynamics and a lattice Boltzmann model to address hydrodynamics to understand the mechanisms of droplet formation in a microfluidic T-junction. They systematically examined the influence of capillary number, flow rate ratio, viscosity ratio, and contact angle in the droplet generation process.

From the available literature, it is clear that the most of the researchers have been focused on the effect of operating variables such as capillary number, flow rates and their ratio, viscosity ratio, etc. However, the understanding of the underlying physics of the droplet formation, in terms of evolution of pressures in both the continuous phase and disperesed phase, in the T-junction is very limited. Garstecki et al. (2006) argued that the dynamics of droplet break-up in a typical T-junction is dominated by the balance of pressures in the dispersed (p_d) and the continuous (p_c) phases at the junction. They drew a heuristic picture of the break-up process, as seen in Fig. 1, and postulated a mechanism based on the assumption that the pressure in the dispersed phase at the inlet remains constant

throughout the break-up process (long-dashed line in Fig. 1e) and explained the process by the evolution of the continuous phase pressure (p_c). Though the assumption essentially reduced the complexity and enabled the process to be explained in simple terms, it did not capture the real scenario. It is because, the dispersed (p_d) and the continuous (p_c) phase pressures are competing against each other at the junction; to explain a scenario during the droplet break-up process, the continuous phase pressure changes while the main channel is blocked by the dispersed phase, then the dispersed pressure will have to change accordingly to remain in the competition and cannot remain constant. Though DeMenech et al. (2008) studied the continuous phase pressure p_c upstream of the T-junction to understand the droplet break-up mechanism from squeezing to dripping and jetting, they did not study the dispersed phase pressure to completely explain the physics of the droplet break-up, in terms of the variation in the pressures of the two phases.

While experimental works have helped to understand underlying physics, experiments at microscale are still difficult. For example, it is very challenging to measure pressure and velocity fields, and droplet size, droplet deformation, break-up and coalescence at such small scales (Liu and Zhang 2009). Therefore, we employ a numerical method to study the dynamics of droplet break-up, especially the evolution of pressures of the continuous and dispersed phases to understand the underlying physics.

2 Numerical simulation

2.1 Geometry of the microchannel

The geometry of the microchannel is shown in Fig. 2a and b. Figure 2a shows the schematic of the three-dimensional rectangular microchannel and Fig. 2b shows the schematic of two-dimensional droplet generation in a microfluidic T-junction. The microchannel dimensions of the main channel are 100 μm in height, 200 μm in width and the length used is 1000 μm and the side channel is 100 μm in width and since the microchannel is planar the height is same as of the main channel (figures not drawn to scale). The dimensions of the channel were chosen keeping in mind the conditions for

geometries that promote squeezing mechanism: (i) the width of the main channel should be greater than its height, and (ii) the width of the inlet channel should be at least equal to half the width of the main channel (Garstecki et al. 2006). The continuous phase (mineral oil) is pumped through the main channel and the dispersed phase (DI water) is pumped through the side channel. The notations p_d in the side channel and p_c in the main channel are for the positions at which the dispersed phase pressure and the continuous phase pressure are measured. These points are located at 50 μm from both the upper and lower walls of the microchannel. (i.e., mid-plane of the three-dimensional channel).

2.2 Governing equations

The transient three-dimensional numerical simulations of the multiphase flow of two immsicible fluids (oil and water) in microchannel with T-junction are performed using VOF method available in the commercial software FLUENT (Ansys Inc. USA). The VOF model can model two or more immiscible fluids by solving a single set of momentum equations and tracking the volume fraction of each of the fluids throughout the domain. The two phases are considered non-interpenetrating. VOF model incorporates the surface tension effects. The flow is considered to be laminar, incompressible, Newtonian, and isothermal with velocity field **V** governed by the Navier–Stokes and continuity equations, which can be written as:

$$\nabla \cdot \mathbf{V} = \mathbf{0} \tag{1}$$

$$\frac{\partial \rho \mathbf{V}}{\partial t} + \nabla \cdot (\rho \mathbf{V}\mathbf{V}) = -\nabla P + \rho g + \nabla \cdot \left(\mu\left(\nabla \mathbf{V} + \nabla^{\mathrm{T}}\mathbf{V}\right)\right) + \mathbf{F}_{\mathrm{s}} \tag{2}$$

Where **V** is the velocity of the mixture, P the pressure, t the time, **F** the volumetric force at the interface resulting from surface tension, ρ the density, and μ dynamic viscosity. In Eq. 2, the accumulation and convective momentum terms in every control volume (cell) balance the pressure force, gravity force, shear force, and additional surface tension force $\mathbf{F}_s$. The physical properties of each fluid are calculated as weighted averages based on the volume fraction of the individual fluid in a single cell. The fluid volume in a cell is

computed as $F_{vol} = FV_{cell,}$ where V_{cell} is the volume of a computational cell and F is the liquid volume fraction in a cell. The value of F in a cell should range between 1 and 0 and $F = 1$ represents a cell which is completely filled with water and $F = 0$ represents a cell which is completely filled with oil and $0 < F < 1$ represents the interface between oil and water.

The liquid volume fraction is determined by solving a separate passive transport equation, given as:

$$\frac{\partial F}{\partial t} + \mathbf{F} \cdot \nabla \mathbf{F} = \mathbf{0} \qquad (3)$$

where,

$$F = \frac{\text{cell volume occupied by water}}{\text{total volume of the control cell}} \qquad (4)$$

The mixture's physical properties are derived from that of the two phases through the volume fraction function. In particular, the average value of ρ and μ in a computational cell can be computed from the value of F in accordance with:

$$\rho = F\rho_2 + (1 - F)\rho_1 \qquad (5)$$

$$\mu = F\mu_2 + (1 - F)\mu_1 \qquad (6)$$

where the subscripts 1 and 2 represent the water and oil phases, respectively.

The governing equations are discretized to algebraic equations by using a control-volume-based technique. The Pressure-Implicit with Splitting of Operators (PISO) algorithm is used in the transient calculations. The technique of Geo-Reconstruct scheme (Piecewise-Linear Interface Construction (PLIC)) is used for the surface tension calculations adopted in this model for the accuracy of the oil– water interface.

The following fluids and their properties were used for both simulations and experiments: (1) mineral oil as the carrier fluid (M5904, Sigma-Aldrich) with 2% w/w Span 80 surfactant (Sigma-Aldrich S6760) and (2) DI water with fluorescent dye (0.05%

w/w Acid Yellow). Hydrodynamic properties: viscosity of DI water (μ) is 1 mPa s, interfacial tension between water and mineral oil is 3.65 mN/m, contact angle between water and PDMS is 115 $^{\circ}$ as the PDMS used in the experiment is hydrophobic and without any surface treatment, viscosity of mineral oil with 2% w/w Span 80 is 23.8 mPa s. Flow rate of deionized water (dispersed phase) was kept constant at 50 μl/h during the experiments and simulations and the capillary number was varied by changing the flow rate of the oil (continuous phase). These fluid properties were set in the fluent properties panel for the fluent VOF simulations. The VOF fluent simulations were run from Ca = 0.008–0.025. Mass flow rate of the continous phase (oil) and the dispersed phase were specified at the inlets according to the capillary number (Ca = $\mu U/\sigma$ where Ca is the capillary number of the flow, μ is the viscosity of the continuous phase, and U velocity of the continuous phase and σ is the interfacial tension between the dispersed phase and the continuous phase) of the flow. Mesh independence study was conducted to ensure the result obtained are independent of the mesh size. Each time step value Δt used in the simulation was 10^{-4} and the Courant number condition was kept at 2.

3 Experimental details

3.1 Fabrication

The channel designs were printed into a photolithographic mask and the negative SU-8 photo resist (MicrochemCorp.) was used to fabricate the master mold using standard procedures specified from Microchem. Then micro-fluidic chips were fabricated using polydimethysiloxane (PDMS) polymer (Dow corning Sylgard 184 Silicone Elastomer) through the standard soft lithography process for PDMS microchannel fabrication (George et al. 2001). The cured PDMS microchannels were bonded to another piece of flat PDMS layer after treating them with oxygen plasma. And they are allowed to recover their hydrophobicity, because of the need of the walls to be hydrophobic which facilitates the formation of water droplets in oil.

3.2 Experimental setup and testing

The continuous phase (oil) and the dispersed phase (deionized water) were pumped from gas-tight syringes (Hamilton, 1.25 ml) through the tubing (0.8 mm PTFE, Cole-Parmer) connected to the inlets, with the help of syringe pumps (KD Scientific, Model No. 781200). Capillary number of the flow was changed by changing the volume flow rate of the continuous phase. The DI water with fluorescent stream forms droplets at the T-junction. The experiments were observed under the Inverted Fluorescence Microscope (Nikon Eclipse TE2000-S) with suitable magnification using Plan Apro objectives. The visualization of the experiments were captured and recorded through the eye piece of the inverted microscope using a high speed camera (1000 FPS) and used for the analysis of the droplet break-up process.

4 Validation of numerical simulation with experimental flow visualization

Simulation results are compared with the experimental results obtained for the same geometry of the microchannel. Figure 3 shows the experimental flow visualization on the left and the simulation results on the right for Ca = 0.01. As can be seen in the figure, the flow visualization of the simulated results for droplet formation match very well with the flow visualization of the experimental results. The process of formation of droplets in the T-junction, as seen in Fig. 3, can be described as follows. The two immiscible fluids (oil and water) form an interface at the junction of the inlet and main channels. The stream of the dispersed phase (water) penetrates into the main channel and a droplet begins to grow; the pressure gradient and the flow in the main channel distort the droplet in the downstream direction. The interface on the upstream side of the droplet moves downstream. When the interface approaches the downstream edge of the inlet for the dispersed phase, the neck connecting the inlet channel with the droplet breaks. The disconnected liquid plug flows downstream in the main channel, while the tip of the stream of the dispersed phase retracts to the end of the inlet and the process repeats. The experimental visualization and the numerical simulation and the process of droplet break-up confirms to the results observed by Garstecki et al. (2006).

5 Pressure profiles in the dispersed and continuous fluids during droplet break-up

Now that we have validated the simulated results with the experimental results and the droplet break-up process confirms to the established results, we can use the pressures measured in the dispersed phase (p_d) and in the continuous phase (p_c) to understand the process of the droplet break-up and the underlying physics. The pressures $p_{d,}$ p_c were measured at positions seen in Fig. 2b. The pressures measured at these positions were recorded over several seconds and the plotted values are a sample of the measured values.

5.1 Squeezing regime

Figure 3 shows the experimental (left) and VOF (right) flow visualizations during the droplet formation process from t = 2.43 s to t = 2.75 s for Ca = 0.01. Figure 4 shows the evolution of pressures in the continuous phase (p_c) and the dispersed phase (p_d) and the difference between (p_d- p_c) them for Ca = 0.01, which falls under the squeezing regime. These two figures are to be referred together to see how $p_{c,}$ p_d and (p_d - p_c) change during the droplet break-up process. We can start from t = 2.43 s when the droplet is about to break as seen in Fig. 3a and b. Figure 3a shows the experimental visualization and 3b shows the VOF computational visualization. This is the final moment of the droplet break-up after squeezing has taken place.

After the droplet break-up, the dispersed phase recoils into the inlet of the side channel and as it recovers the pressure for the next cycle, its pressure p_d jumps up to a higher level; but pressure p_c comes down because the droplet, after the break-up, moves down with the flow and provides less resistance to the flow of the continuous phase. Therefore, the difference between p_d and p_c reaches the maximum before the start of the next cycle as seen in Fig. 4(I). Now, during the start of the droplet formation process, the dispersed phase starts to push itself into the main channel and the pressure p_d slowly comes down. But the continuous phase pressure p_c starts climbing slowly to adjust to the incoming dispersed phase which increasingly occupies more area as the

droplet formation process proceeds. The sudden fall in pressure for both p_d and p_c, between t = 2.63 s and t = 2.54 s, is due to a droplet, which had been formed before, leaving the channel at the outlet. This is because the pressure drop across the channel is dependent on the number of droplets in the channel (Fuerstman et al. 2007). Once the droplet leaves the outlet both p_d and p_c regain their pressure. But the difference between, p_d - p_c, slowly decreases as the droplet emerges from the side channel into the main channel.

In the blocking phase—where the dispersed phase starts blocking (Figs. 3g, 4 (II)) the main channel significantly and spans the whole cross-section of the main channel ($\varepsilon << w$)—p_d gradually decreases as the dispersed is pushed into the main channel and p_c increases to the point. In this stage, p_d - p_c declines linearly with a steep slope and the process proceeds to the squeezing stage (Figs. 3i, j, 4 (III)). In the squeezing stage, as the droplet elongates in the downstream direction and the neck connecting it to the inlet thins p_d - p_c remains almost constant, and paving the way for the continuous pushing of the dispersed phase till the final stage of break-up happens (Figs. 3m, n, 4 (IV)). At this point, both p_d and p_c come down and their difference p_d - p_c is at the lowest value, unlike suggested by other researchers that it happens between the second and third stage of the droplet formation process (Garstecki et al. 2006).

From the above observation, four stages of droplet formation can be identified in terms of the pressure difference p_d - p_c as seen in Fig. 4: entering stage (I), where p_d - p_c decreases slowly; blocking stage (II), where p_d- p_c decreases steeply; elongation stage (III), where p_d- p_c remains almost constant; droplet break-up stage (IV), where p_d - p_c reaches the lowest point.

After the break-up, the dispersed phase recoils back to the inlet and the above described process repeats. Fluctuations in p_d and p_c are clearly seen throughout the droplet formation process in Fig. 4. The reason for fluctuations in p_d and p_c can be explained as follows: as the droplets tracked in the flow is comparable to the size of the channel, they block and provide resistance to the flow of the dispersed phase. As these droplets are moving and are coupled to the flow in momentum and continuity equation, the competition between the two phases leads to fluctuations in both p_d and p_c. In

incompressible fluids pressure disturbances are transmitted instantly and therefore, fluctuations in p_d- p_c is less compared to the individual pressure fluctuations.

5.2 Transition regime

Figures 5 and 6 show the pressures, p_d and p_c, measured and the difference p_d - p_c for Ca = 0.014 and Ca = 0.018, respectively. Figure 7 shows the experimental (left) and numerical (right) flow visualizations for Ca = 0.018. It can be seen that the experimental visualizations match to the VOF simulated visualizations. In the transient regime, the dynamics of droplet break-up is dominated by both the shear force and the squeezing mechanism. The dispersed fluid from the side channel blocks the main channel partially and the size of the droplet produced is significantly smaller than in the squeezing regime. The time required for droplet formation is also reduced as the capillary number is increased. It can be observed from Figs. 4, 5, and 6 that, as the capillary number increases, the length of the pressure curve for the dispersed phase p_d and the time required for recoiling and and regaining the pressure for the next cycle slowly decreases. This is because the velocity of the fluid and the shear stress it exerts on the incoming fluid from the dispersed phase increases with increase in capillary number; the squeezing phenomenon gradually starts disappearing—not an abrupt change, but gradual—until the droplet formation process moves to the dripping regime. This happens along with the increase in the pressures of p_d and p_c. The individual pressures of p_d and p_c at higher capillary numbers may be high but the pressure difference between them remains almost constant as seen in Fig. 11. In the transition regime, the stages of droplet formation cannot be clearly distinguished in terms of the pressure difference p_d - p_c, as in the squeezing regime, because of almost a linear decline as seen in Figs. 5 and 6. The lowest difference for p_d - p_c happens at the moment of droplet break-up (Fig. 8).

5.3 Dripping regime

In the dripping regime, where the role of shear stresses becomes more important, the contribution by the pressure build up to droplet break-up becomes lower but nevertheless exist and never becomes negligible, unless the radius of the droplet is much smaller than

the width of the channel (DeMenech et al. 2008). But in the confined channel the droplet size is comparable to the size of the microchannel and the droplet break-up occurs due to both shear stress and pressure build-up. Figure 10 shows both the experimental (left) and the VOF flow visualizations (right) for Ca = 0.025, where the process of droplet formation and the break-up with respect to time can be referred together with Fig. 9. The droplet clearly does not occupy the main channel fully as in the squeezing regime as seen in Fig. 10 and the volumetric rate of flow of the continuous phase makes it to flow faster in gap between the droplet and the wall of the channel and exerts a larger shear stress on the droplet. And the size of droplet in this regime is comparatively lower than in the squeezing and the transition regime.

The fluctuations in the pressure of both dispersed and continuous phase in the dripping regime decrease as the capillary number increases. This result is consistent with the observation made by DeMenech et al. (2008). During the droplet formation process, after the pressure recovery, p_d continues to decrease and p_c continues increase till they reach the point where the droplet breaks up. The sudden drop in both p_d and p_c is due to a droplet leaving the channel exit as explained in the squeezing regime. In the dripping regime, the pressure difference p_d - p_c decreases in a linear fashion and the stages of droplet formation cannot be identified, as is the case for this regime.

5.4 Effect of Ca on p_d - p_c

Figure 11 shows the difference between the pressures measured in the dispersed phase and continuous phase p_d- p_c for capillary numbers between 0.01 and 0.025. As seen in Fig. 11, the difference in the pressures are bounded within a range and does not vary much with the increase in capillary number. The time for forming a droplet decreases as the capillary number increases. This result is similar to the results obtained by DeMenech et al. (2008). They observed that for a fixed viscosity ratio as the capillary number increases parameters such as squeezing time remains unchanged. Therefore, the characteristics that the pressure difference remains for a wide range of capillary number could be attributed to the viscosity ratio, i.e., for a given viscosity ratio the pressure difference required to form droplets in a wide range of capillary numbers remains

constant.

6 Conclusions

Our numerical investigation of the dynamics of droplet break-up in the T-junction of a microchannel has revealed that the evolution of pressure in the dispersed phase varies as much as the continuous phase pressure in the squeezing regime, transition regime and in the dripping regime. The evolution of pressure over time in the continuous phase and the flow visualization confirms to the model proposed by other researchers. Therefore, the pressure measured in the dispersed phase represents the true picture of the droplet break-up process in a microfluidic T-junction. From the variation of the dispersed phase pressure we could see that the assumption of constant dispersed phase pressure leads to an unrealistic picture, though it allowed to explain the droplet formation process in simple terms. The difference between the dispersed phase pressure and the continuous phase pressure shows us that the droplet formation process in a T-junction starts with a higher pressure difference and as the process proceeds to form a droplet the difference reduces gradually as the droplet formation proceeds. The lowest difference between the p_{d} and p_{c} happens at the moment of droplet break-up, and not between the second and third stage of the droplet formation process as suggested by other researchers. The findings of this study are important for multiphase microfluidics, as the understanding of droplet formation and the physics behind the process are essential for designing integrated multiphase micro-fluidic systems.

References

Bringer MR, Gerdts CJ, Song H, Tice JD, Ismagilov RF (2004) Microfluidic systems for chemical kinetics that rely on chaotic mixing in droplets. Philos Trans Math Phys Eng Sci A 362(1818):1087–1104

DeMenech FJM, Garstecki P, Stone H (2008) Transition from squeezing to dripping in a microfluidic T-shaped junction. J Fluid Mech 595:141–161

Fuerstman MJ, Lai A, Thurlow ME, Sergey HAS, Shevkoplyas S, Whitesides GM (2007) The pressure drop along rectangular microchannels containing bubbles. Lab Chip 7:1479–1489

Garstecki P, Fuerstman MJ, Stone HA, Whitesides GM (2006) Formation of droplets and bubbles in a microfluidic T-junction— scaling and mechanism of break-up. Lab Chip 6(3):437–446

George EO, Whitesides M, Takayama S, Jiang X, Ingber DE (2001) Soft lithography in biology and biochemistry. Ann Rev Biomed Eng 3:335–373

Gordon JAT, Christopher F, Noharuddin NN, Anna SL (2008) Experimental observations of the squeezing-to-dripping transition in T-shaped microfluidic junctions. Phys Rev 78:036317

Guillot P, Colin A (2005) Stability of parallel flows in a microchannel after at junction. Phys Rev E 72:066301

Gunther A, Khan SA, Thalmann M, Traschel F, Jensen K (2004) Transport and reaction in microscale segmented gas–liquid flow. Lab Chip 4:278–286

Gunther A, Khan SA, Thalmann M, Trachsel F, Jensen KF (2004) Transport and reaction in microscale segmented gas-liquid flow. Lab Chip 4(4):278–286

Gunther A, Jhunjhunwala M, Thalmann M, Schmidt MA, Jensen KF (2005) Micromixing of miscible liquids in segmented gas–liquid flow. Langmuir 21(4):1547–1555

Liu H, Zhang Y (2009) Droplet formation in a T-shaped microfluidic junction. J Appl Phys 106:034906

Long Sang YH, Wang F (2009) Investigation of viscosity effect on droplet formation

in T-shaped microchannels by numerical and analytical methods. Microfluid Nanofluid 6:621–635

Muradoglu M, Stone HA (2005) Mixing in a drop moving through a serpentine channel: a computational study. Phys Fluids 17(7):1–9

Nisisako T, Okushima S, Torii T (2005) Controlled formulation of monodisperse double emulsions in a multiple-phase microfluidic system. Soft Matter 1(1):23–27

Sivasamy J, Chim YC, Wong T-N, Nguyen N-T, Yobas L (2010) Reliable addition of reagents into microfluidic droplets. Microfluid Nanofluid 8:409–416

Song H, Bringer MR, Tice JD, Gerdts CJ, Ismagilov RF (2003) Experimental test of scaling of mixing by chaotic advection in droplets moving through microfluidic channels. Appl Phys Lett 83(22):4664–4666

Song H, Chen DL, Ismagilov RF (2006) Reactions in droplets in microfluidic channels. Angew Chem Int Ed 45(44):7336–7356

Squires TM, Quake SR (2005) Microfluidics: Fluid physics at the nanoliter scale. Rev Mod Phys 77(3):977–1026

Stone HA, Stroock AD, Ajdari A (2004) Engineering flows in small devices: microfluidics toward a lab-on-a-chip. Annu Rev Fluid Mech 36:381–411

Teh S, Lin R, Hung L, Lee AP (2008) Droplet microfluidics. Lab Chip 8(2):198–220

Thorsen T, Roberts RW, Arnold FH, Quake SR (2001) Dynamic pattern formation in a vesicle-generating microfluidic device. Phys Rev Lett 86(18):4163–4166

Tice JD, Lyon AD, Ismagilov RF (2004) Effects of viscosity on droplet formation and mixing in microfluidic channels. Anal Chim Acta 507(1):73–77

Utada AS, Lorenceau E, Link DR, Kaplan PD, Stone HA, Weitz DA (2005) Monodisperse double emulsions generated from a microcapillary device. Science 308(5721):537–541

Xu JTJH, Li SW, Luo G (2008) Correlations of droplet formation in T-junction microfluidic devices: from squeezing to dripping. Microfluid Nanofluid 5:711–717

Zheng B, Ismagilov RF (2005) A microfluidic approach for screening submicroliter volumes against multiple reagents by using preformed arrays of nanoliter

plugs in a three-phase liquid/ liquid/gas flow. Angew Chem Int Ed 44(17):2520–2523

List of Figures

stream blocks the main channel, (*III*) the droplet elongates and grows downstream, (*IV*) the droplet break-up

Fig. 5 Evolution of pressures in the continuous phase p_c and the dispersed phase p_d and the difference between them (p_d- p_c) for Ca= 0.014

Fig. 6 Evolution of pressures in the continuous phase p_c and the dispersed phase p_d and the difference between them (p_d - p_c) for Ca = 0.018

Fig. 7 Snapshots of flow visualizations: experimental (*left*) and the VOF simulation (*right*) for Ca= 0.018

Fig. 8 Evolution of pressures in the continuous phase p_c and the dispersed phase p_d and the difference between them (p_d - p_c) for Ca = 0.022

Fig. 9 Evolution of pressures in the continuous phase p_c and the dispersed phase p_d and the difference between them (p_d - p_c) for Ca =0.025

Fig. 10 Snapshots of flow visualizations: experimental (*left*) and the VOF simulation (*right*) for Ca = 0.025

Fig. 11 Effect of Ca on the difference of dispersed phase and continuous phase pressures (p_d - p_c)

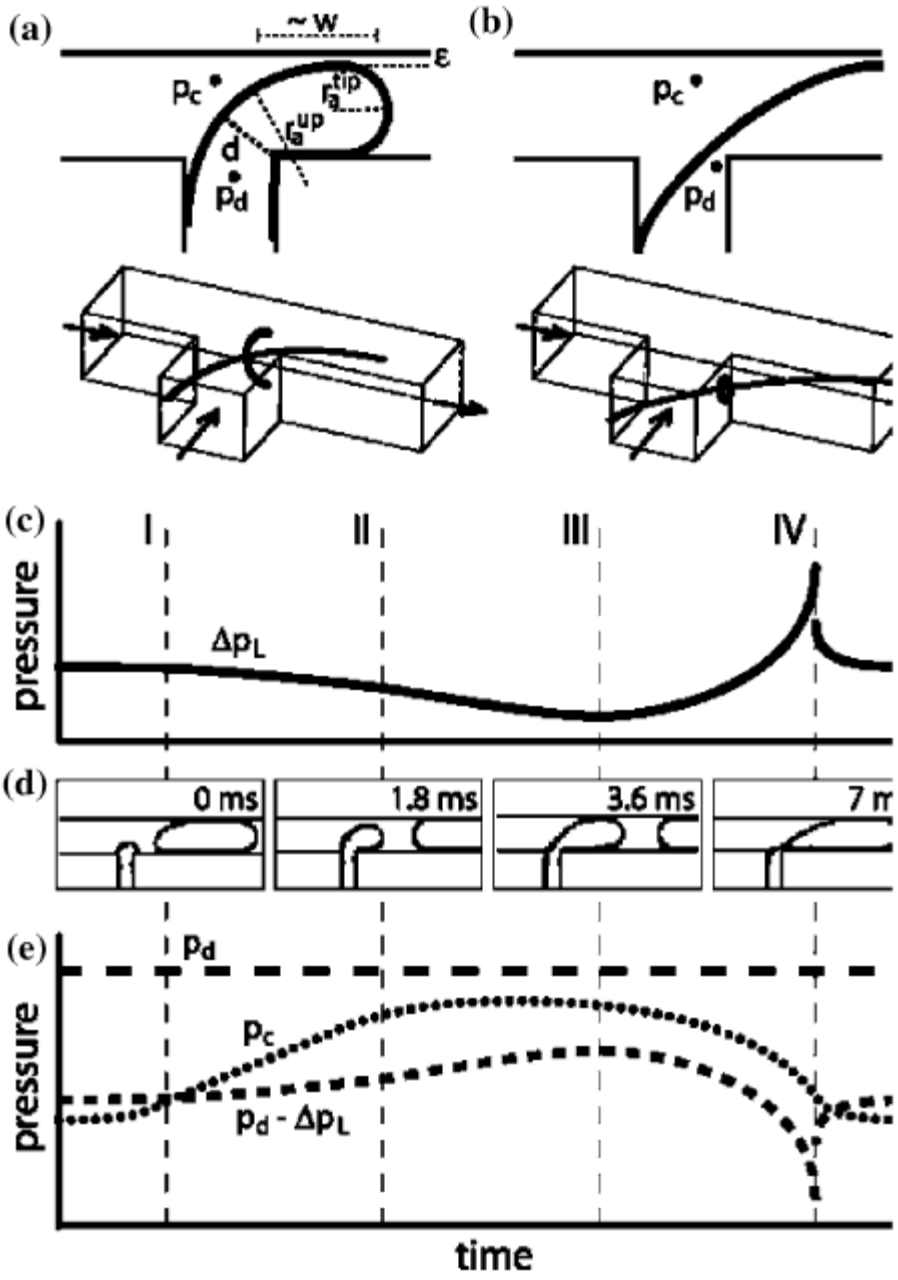
(a)
~w
ε
p_c
r_a^{tip}
r_a^{up}
d
p_d
(b)
p_c
p_d
(c)
I
II
III
IV
pressure
Δp_L
(d)
0 ms
1.8 ms
3.6 ms
7 m
(e)
p_d
p_c
$p_d - \Delta p_L$
pressure
time

Fig. 1

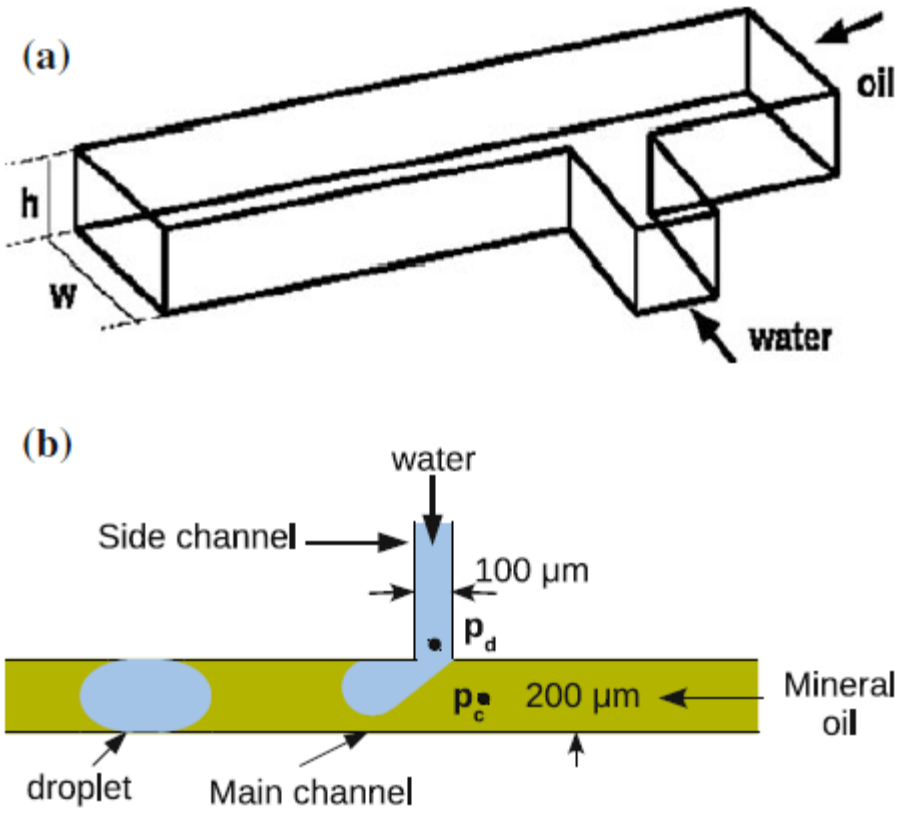
(a)
oil
h
w
water
(b)
water
Side channel
100 µm
p_d
p_c
200 µm
Mineral oil
droplet
Main channel

Fig. 2

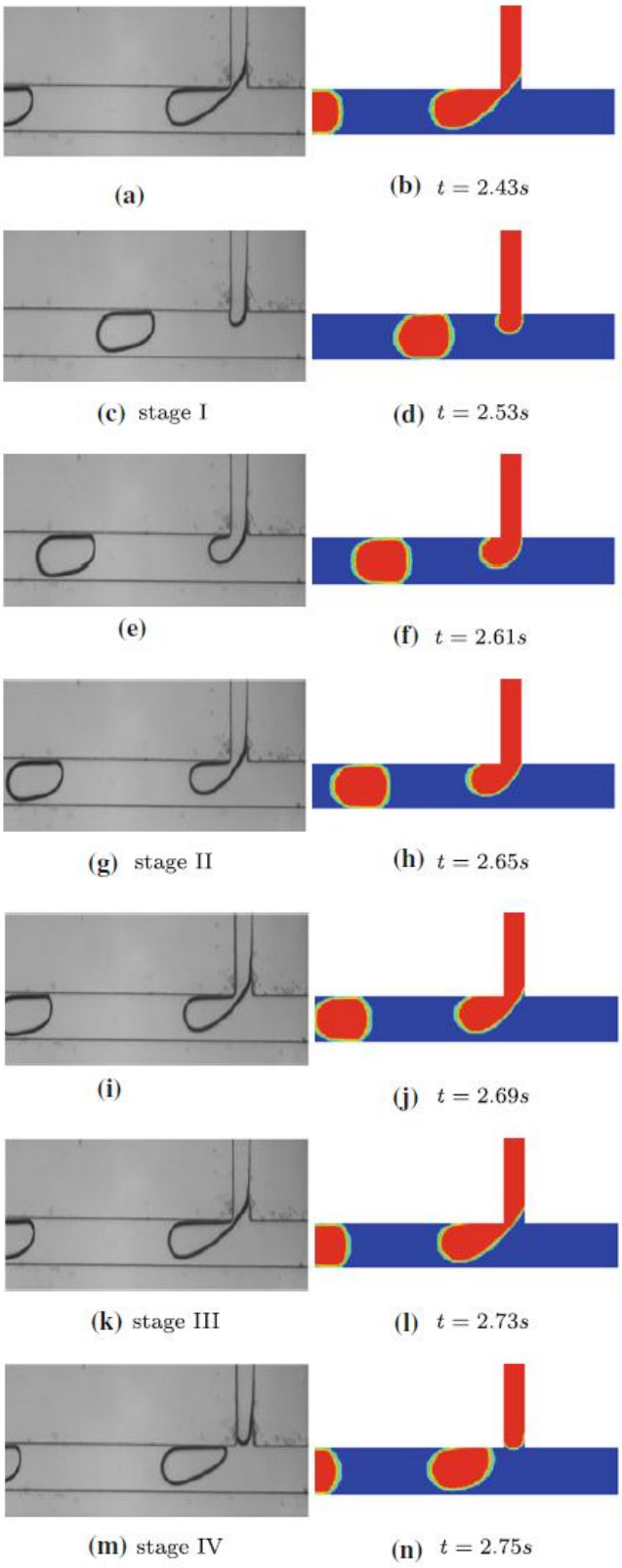
(a)
(b) $t = 2.43s$
(c) stage I
(d) $t = 2.53s$
(e)
(f) $t = 2.61s$
(g) stage II
(h) $t = 2.65s$
(i)
(j) $t = 2.69s$
(k) stage III
(l) $t = 2.73s$
(m) stage IV
(n) $t = 2.75s$

Fig. 3

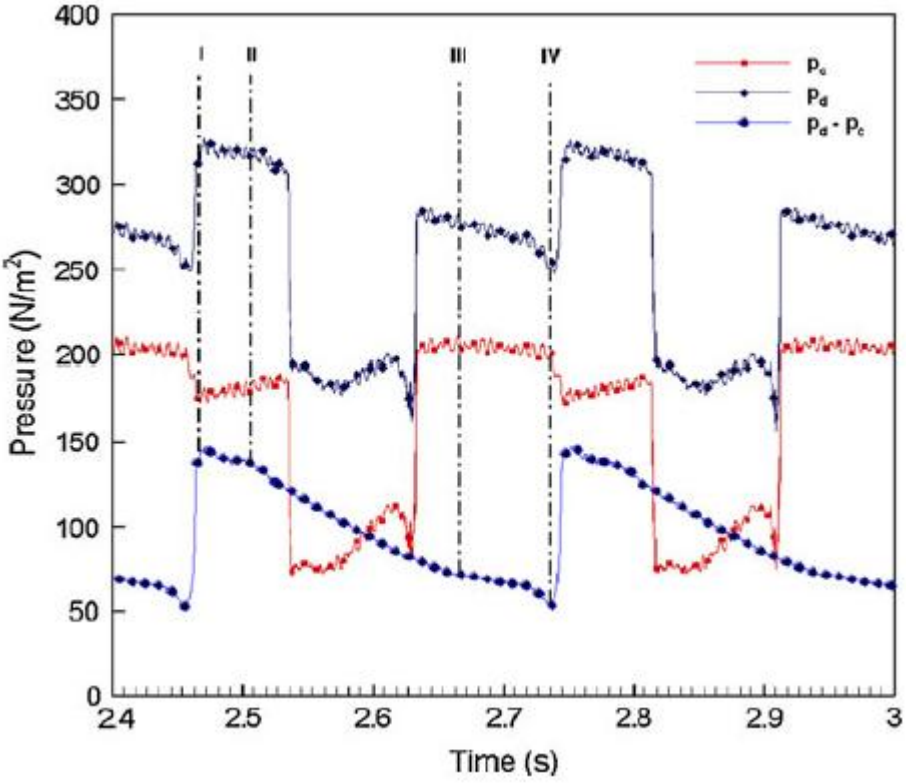
400
350
300
250
200
150
100
50
0
Pressure (N/m²)
I
II
III
IV
Pc
Pd
Pd - Pc
2.4
2.5
2.6
2.7
2.8
2.9
3
Time (s)

Fig. 4

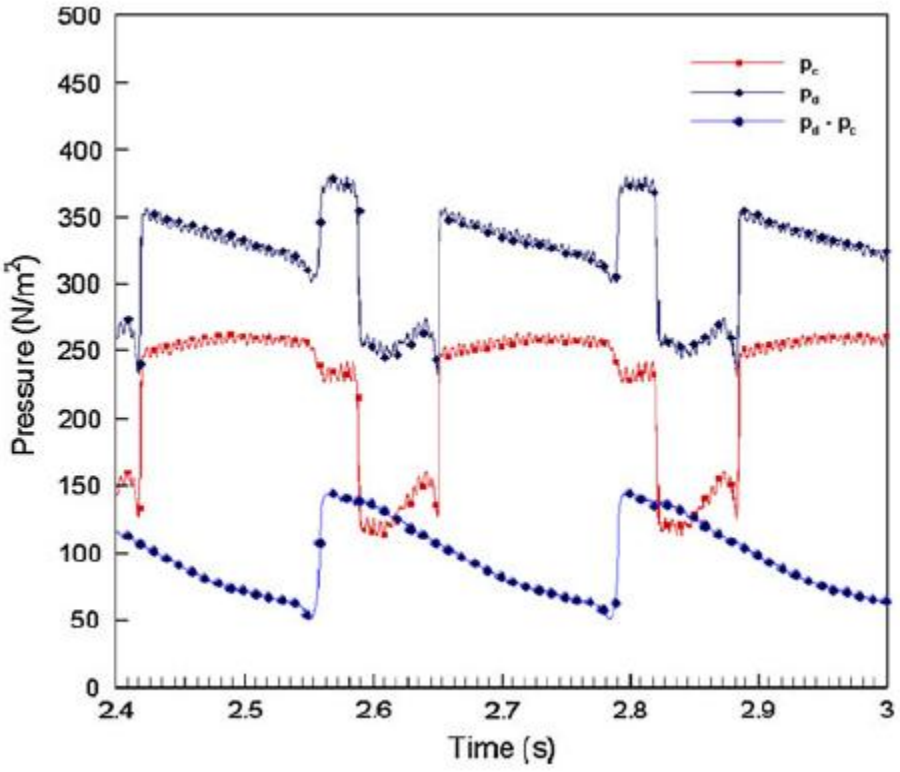
500
450
400
350
300
250
200
150
100
50
0
Pressure (N/m²)
2.4
2.5
2.6
2.7
2.8
2.9
3
Time (s)
p_c
p_d
$p_d - p_c$

Fig. 5

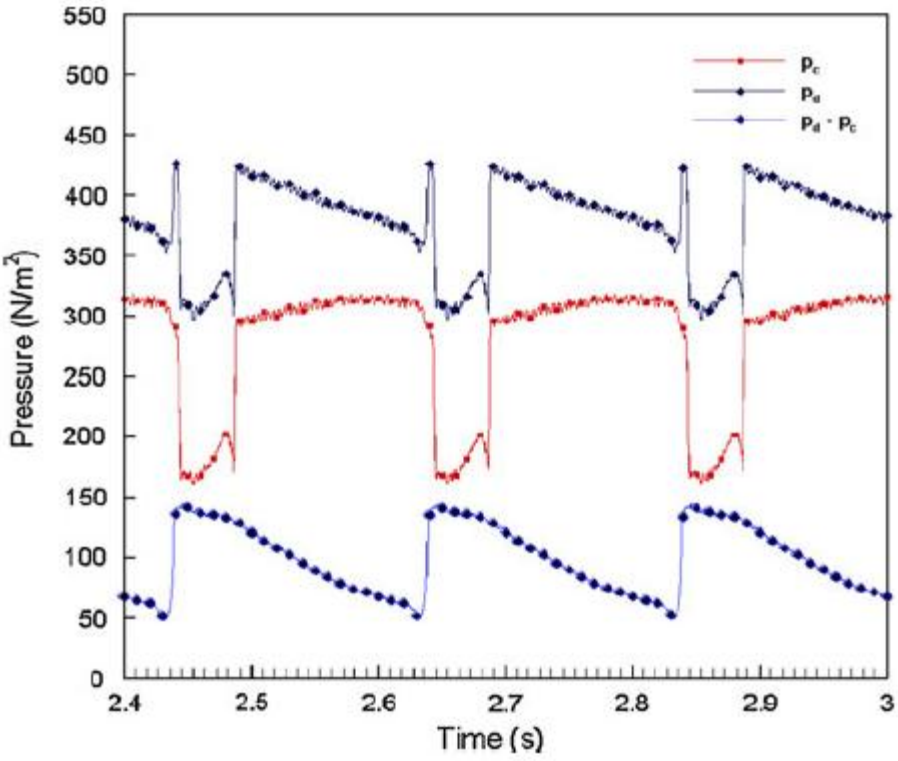
550
500
450
400
350
300
250
200
150
100
50
0
Pressure (N/m²)
2.4
2.5
2.6
2.7
2.8
2.9
3
Time (s)
Pc
Pd
Pd - Pc

Fig. 6

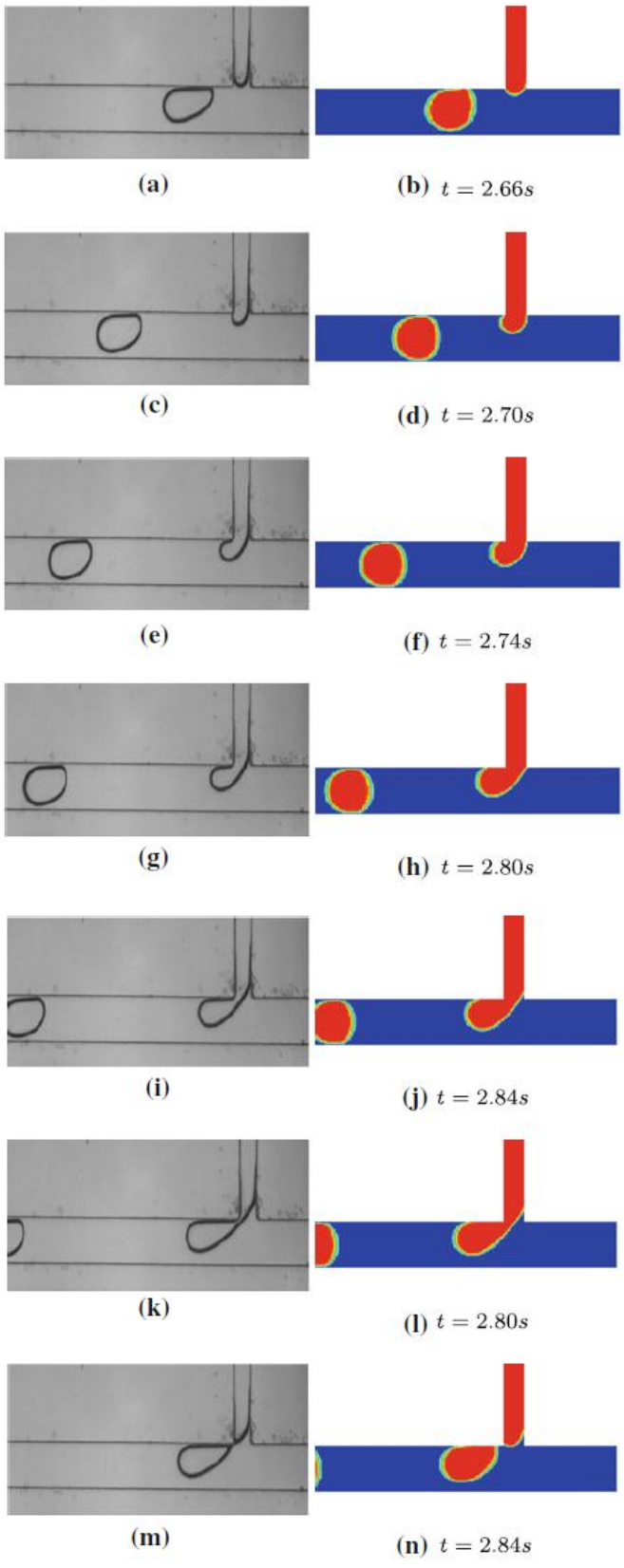

Fig. 7

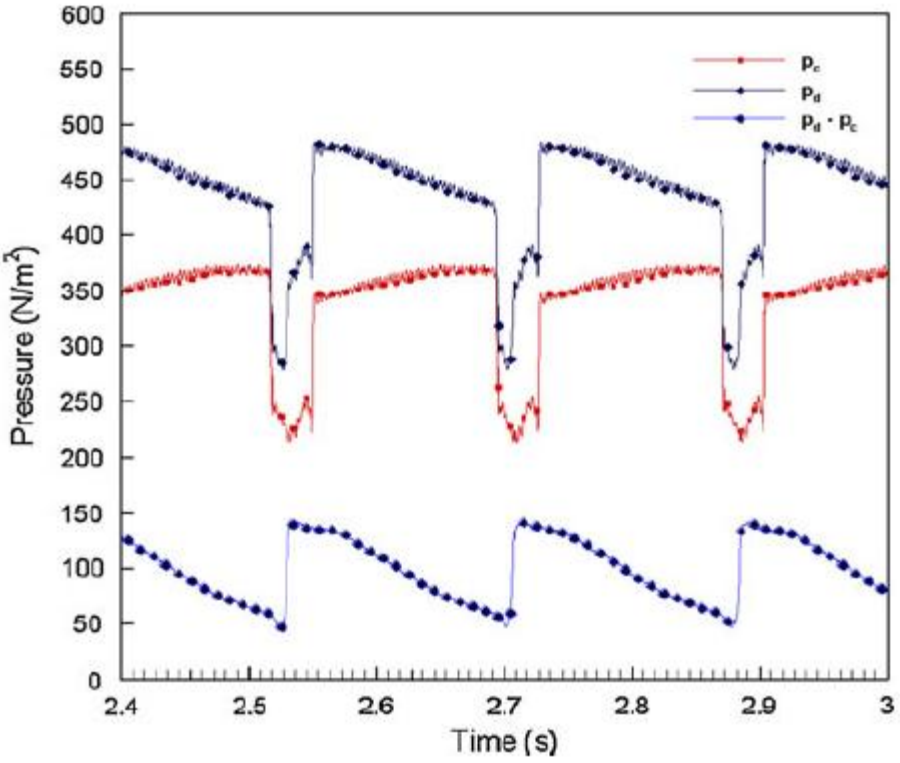
600
550
500
450
400
350
300
250
200
150
100
50
0
Pressure (N/m²)
2.4
2.5
2.6
2.7
2.8
2.9
3
Time (s)
Pc
Pd
Pd - Pc

Fig. 8

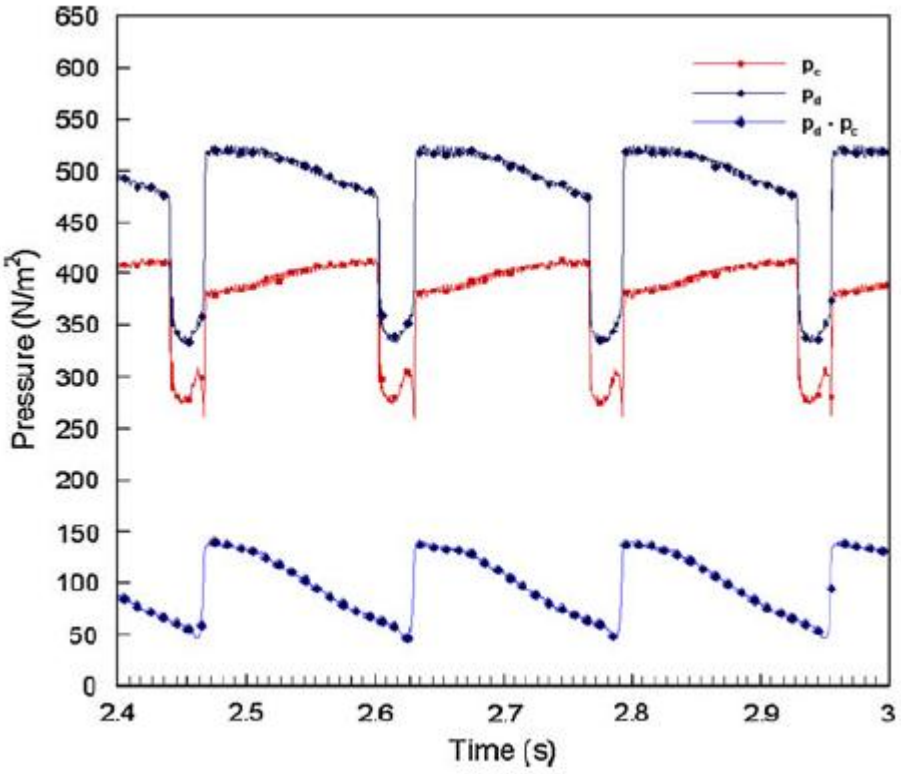
650
600
550
500
450
400
350
300
250
200
150
100
50
0
Pressure (N/m²)
2.4
2.5
2.6
2.7
2.8
2.9
3
Time (s)
p_c
p_d
p_d - p_c

Fig. 9

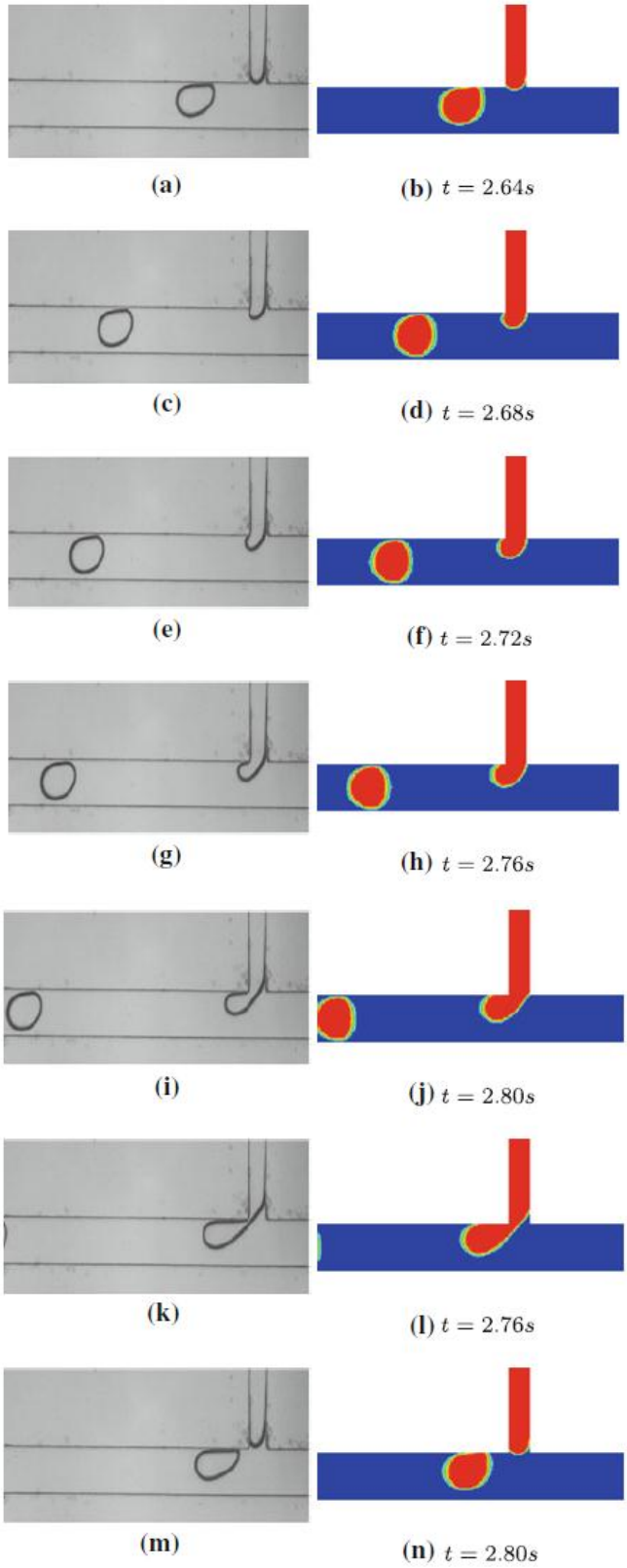

Fig. 10

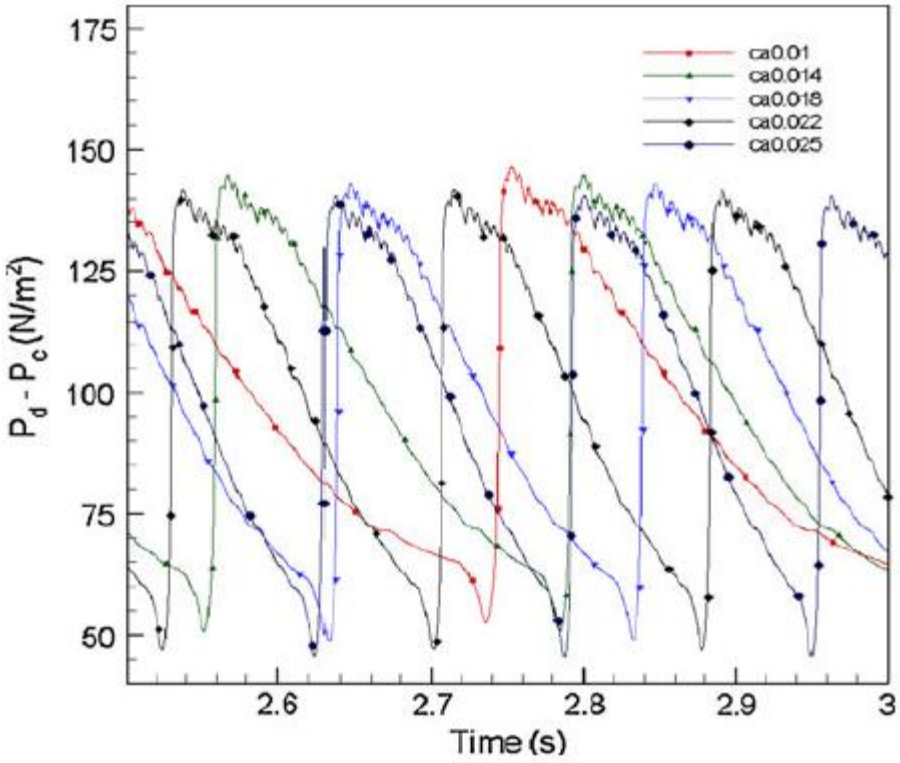
175
150
125
100
75
50
2.6
2.7
2.8
2.9
3
Time (s)
$P_d - P_c (N/m^2)$
ca0.01
ca0.014
ca0.018
ca0.022
ca0.025

Fig. 11